Radar Imaging Approach for Zero-Power Millimeter-Wave Wireless Sensors

Dominique Henry, Hervé Aubert, Patrick Pons

Radar Imaging Approach for Zero-Power Millimeter-Wave Wireless Sensors

Dominique HENRY
MINC department
LAAS-CNRS
Toulouse, France
dhenry@laas.fr

Hervé AUBERT
MINC department
LAAS-CNRS
Toulouse, France
haubert@laas.fr

Patrick PONS
MINC department
LAAS-CNRS
Toulouse, France
ppons@laas.fr

***Abstract*—This paper reports a new technique for detecting and remotely analysing zero-power (or fully passive) and wireless sensors. It consists of segmenting with isolines three-dimensional radar images provided by Frequency-Modulated Continuous-Wave radars. An isoline refers here to a line along which the radar echo amplitude is the same. Recent applications of this technique on temperature and humidity zero-power sensors are reported.**

***Index Terms*—passive sensors, chipless sensors, radar imaging, millimeter-wave, clutter mitigation techniques**

I. Introduction

Zero-power (or passive, battery-less), wireless and chipless sensors are very good candidates for remotely measuring physical quantities in harsh environment (e.g., in high radiation or extreme temperature conditions) and/or for applications requiring sensing devices with low-cost of fabrication, small size and long-term measurement stability [1]. These devices convert usually the variation of a physical quantity (such as, e.g., pressure or temperature) into the measurable variation of an electromagnetic wave descriptor, such as, the radar echo level of sensors [2]. In 2008 [3], we proposed to use well-known FMCW (Frequency-Modulated Continuous-Wave) radars for remotely interrogating fully passive and wireless sensors and since that date, the use of such radars to passive sensors interrogation has grown steadily. Over the last decade, the increasing development of easy-to-use millimetre-wave (mm-wave) FMCW radars has intensified their application in Wireless Sensor Network and Internet of Things related applications. At first reserved for automotive applications, these radars are now commercialized for industrial applications in ISM (Industrial, Scientific and Medical) frequency bands [4]. High frequencies of operation allow designing large modulation bandwidth (and consequently, high depth resolution [5]) and compact antennas for integrated MIMO (Multiple Inputs Multiple Outputs) front-ends [6]. Commercially available mm-wave radars offer new opportunities, such as, the intra-parcel radar imaging in precision viticulture [7], [8] and the monitoring of livestock behavior [9].

In this paper, we report a new technique for detecting and remotely analyzing fully passive wireless sensors. It consists of segmenting with isolines (or iso-echo lines) the three-dimensional images provided by mm-wave FMCW radars. An isoline refers here to a line along which the radar echo amplitude is the same. Recent applications to temperature and humidity zero-power sensors are reported and discussed here.

II. 3D Radar Imaging Technique for Wireless Sensors : Principle

A. Passive and wireless sensors

A fully passive (or zero-power), wireless and chipless sensor may be modeled as an antenna of input impedance Z_{ANT} loaded by a so-called sensing impedance $Z(\Phi)$, whose value is assumed to be dependent on the physical quantity Φ of interest. Examples of such sensing devices are provided by, e.g., pressure [10]–[12] nuclear radiation [13], gas [14], temperature [15]–[19] and strain [20] sensors. The remote measurement of the physical quantity Φ from the analysis of the radar echo variability of sensors was originally proposed in [3], while the proof-of-concept was demonstrated for the first time in [21] by using a mm-wave FMCW radar.

As displayed in Fig. 1(a), a transmission line of electrical length L characteristic impedance Z_0 can be eventually added between the antenna and the sensing impedance Z in order to: (i) discriminate between the sensing (or antenna) scattering modes and the structural scattering mode [22], (ii) enhance the mitigation of radar clutter [23] and/or (iii) identify passive and chipless sensors in wireless network applications [24] (the identification of such sensors can also be performed without adding transmission lines, but from using reconfigurable multi-band scatterers [25], [26]).

Let $P_r(Z)$ be the electromagnetic power reflected by the impedance $Z(\Phi)$ when the fixed power P_{inc} is injected in the impedance through a transmission line. When Z is close to the matched impedance, the reflected power $P_{r,min}$ is very small, and when Z is very small or very large compared with the matched impedance, the reflected power takes its maximal value $P_{r,max}$. Maximal achievable full-scale range Δ_{max} for the reflected power is defined by $P_{r,max} - P_{r,min}$. Next, let $Z_A = Z(\Phi_A)$ be the impedance for which the reflected power takes its smallest value $P_{r,A}$ and let $Z_B = Z(\Phi_B)$ be the impedance for which the reflected power takes its maximal value $P_{r,B}$. The full-scale range Δ is then given by $P_{r,B} - P_{r,A}$. As illustrated in Fig. 1(b), one could target the design of the so-called *ideal* sensing device for which (i) the reflected

978-1-7281-0589-5/19/$31.00

power varies linearly with respect to the physical quantity Φ, and (ii) the full-scale range Δ reaches the maximal achievable full-scale range Δ_{max}. With such *ideal* sensing device, the relationship between the reflected power P_r and the physical quantity Φ would be bijective for $\Phi_B < \Phi < \Phi_A$ (assuming $\Phi_B < \Phi_A$), and the full-scale measurement range would be as high as possible. However, the design of such sensing device is very challenging and in practice, due to the lack of a generic design methodology, efforts are still undertaken on a case-by-case basis for both increasing the full-scale measurement range Δ and enhancing the sensor linearity of passive sensors.

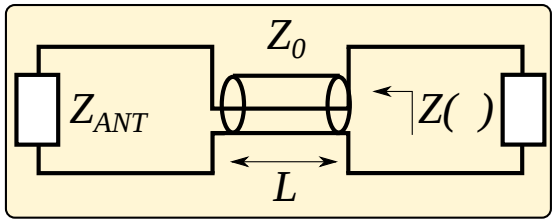

(a)

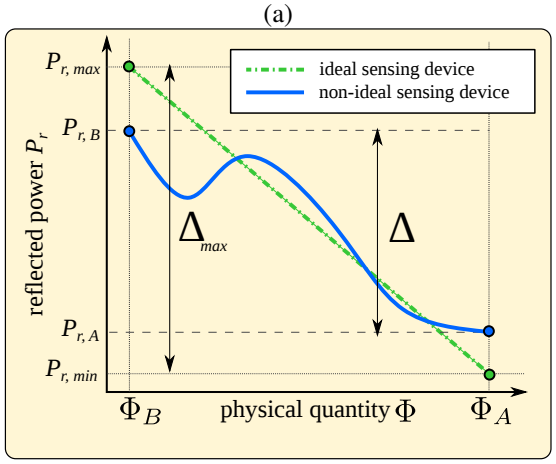

(b)

Fig. 1. (a) Schematic of passive and wireless sensors loaded by sensing impedance $Z(\Phi)$, (b) Power reflected by the sensing impedance as a function of the physical quantity Φ when the fixed power P_{inc} is injected in the impedance for the *ideal* (in green) and *non ideal* (in blue) sensor designs.

B. Wireless reading of passive sensors from the beat frequency spectrum provided by FMCW radar

The signal or *chirp* transmitted by the FMCW radar in the sensor direction has typically a linear sawtooth variation of frequency over time. The chirp with carrier frequency f_C , bandwidth (or excursion frequency) B, and sawtooth modulation period T_R is then backscattered by the sensor and next, it is received by the radar Rx-antenna. The Fast Fourier Transform of the signal resulting from the mixing of the received and transmitted chirps, is called the *beat frequency spectrum* [27]. From this spectrum, which gives radar echo magnitudes along the direction of the sensor as a function of the distance from the radar, the radar-to-sensor separation distance can be derived, with a theoretical depth resolution given by $\frac{c}{2B}$ where c is the speed of light. In the beat frequency spectrum, the so-called *structural* and the *sensing* (or *antenna*) scattering modes generated by the illuminated passive sensor can be detected [28], [29]. Inserting the optional electrical length L of transmission line between the antenna and the sensing impedance $Z(\Phi)$ allows controlling the separation distance between these two scattering modes in the beat frequency spectrum.

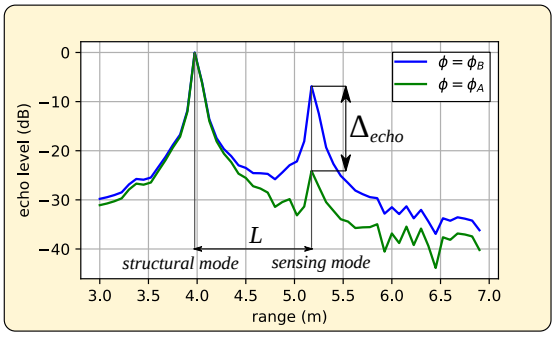

Fig. 2. Simulated beat frequency spectra of a passive sensor located at distance of 4.0m in front of the radar for $\Phi = \Phi_A$ (green curve) and $\Phi = \Phi_B$ (blue curve).

Fig. 2 displays the beat frequency spectrum of a simulated passive sensor with L=1.2m placed at a distance of 4.0m in front of a FMCW radar and for two different values of the physical quantity: $\Phi = \Phi_A$ (in green) and $\Phi = \Phi_B$ (in blue). As expected, the magnitude of the structural scattering mode (detected at 4.0m) does not depend on Φ, while the magnitude of the sensing scattering mode (detected at 5.2m) varies when Φ changes : for $\Phi = \Phi_A$, the power $P_{r,A}$ reflected by the impedance Z_A is low and the corresponding echo level detected at 5.2m is small (–25dB), while for $\Phi = \Phi_B$, the reflected power $P_{r,B}$ is larger and it is then associated with a significantly higher echo level (–7dB). For narrow bandwidth B, it has been recently shown that the full-scale range Δ_{echo} for the echo level is linearly dependent on the full-scale range Δ for the reflected power [30]. Moreover, the lower the signal-to-noise ratio, the narrower the full-scale range Δ_{echo}. Last but not least, large full-scale range Δ_{echo} may be obtained when the main lobe of the directive Tx-antenna of the radar points into the direction of the sensor. However, when this lobe slightly deviates from the sensor direction, an abrupt reduction of the full-scale range Δ_{echo} is observed. This lack of robustness is a major issue when analyzing the beat frequency spectrum obtained in the sensor direction only. To solve this problem, a solution based on three-dimensional (3D) radar imaging approach was proposed for the first time in 2015 [31]–[33] and is described in the next section.

C. Wireless reading of passive sensors from 3D radar images

The full-scale range Δ_{echo} for the echo level of passive sensors reported in Section II-B was obtained from the analysis of the beat frequency spectrum obtained in the sensor direction, and only in this direction. However, this range is not guaranteed in practice, because the main lobe of the radar Tx-antenna may not point in the sensor direction. To overcome this problem, we propose to perform a 3D beamscanning of

the scene in order to analyze multiple beat frequency spectra in different directions in space. Each beat frequency spectrum is associated to a specific angular direction (θ, φ), where θ denotes the elevation angle and φ denotes the azimuth angle. Thus, the radar provides three-dimensional images with elevation, azimuth and range coordinates.

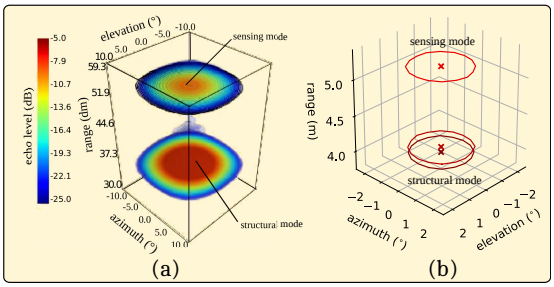

Fig. 3. (a) Simulated 3D radar echoes from a passive sensor located at 4.0m in front of the radar and for $\Phi = \Phi_B$. The echoes are represented by using isosurfaces, i.e., surfaces of same echo level in azimuth/elevation/range coordinates; (b) Computed isolines for the echo level threshold t_{init} = –10dB.

For the sake of illustration, the simulation of a 3D radar beamscanning is performed here with the passive sensor used in Section II-B. The Tx-antenna of the radar (beamwidth of 4°) is swept from -10° to 10° in azimuth and elevation. The 3D radar echo associated with the sensing scattering mode can then be visualized by using isosurfaces [34]. Isosurfaces are surfaces of same echo level in azimuth/elevation/range coordinates. The 3D radar echoes of the simulated passive sensor are displayed in Fig. 3(a) for $\Phi = \Phi_B$. Red colors indicate isosurfaces for higher echo level, while blue colors show isosurfaces for lower echo level. Isosurfaces associated with the structural scattering mode are detected at 4.0m with a strong echo level; isosurfaces associated with the sensing scattering mode are detected at 5.2m. These 3D radar echoes are segmented by so-called isolines in each plane (θ, φ). The isolines are generated by an algorithm described in [8] starting with an echo threshold t_{init} . Inside each specific isoline is included one unique local maximum of echo level. Such isolines are displayed in Fig. 3(b) for t_{init} = –10dB. Three isolines can be isolated: the two isolines at 4.0m (bottom of the graph) are associated with the structural scattering mode, while the isoline at 5.2m (top of the graph) is associated with the sensing scattering mode for $\Phi = \Phi_B$. Statistical estimators can be defined from this isoline in order to derive the value of the physical quantity Φ. The isolines of the sensing scattering mode at 5.2m are simulated and displayed in Fig. 4(a) for physical quantity Φ varying between Φ_A and Φ_B. We define the statistical estimator e_{Max} as the maximal echo level inside the isoline. e_{Max} is displayed in Fig. 4(b) for various values of Φ. Each point in the graph represents e_{Max} of each isoline of Fig. 4(a) and for the same value of Φ. Using this estimator, we obtain a large full-scale range Δ_{echo} of 23.7dB. Several other estimators may be defined from isolines [35], each having its specific characteristics in terms of linearity and full-scale range.

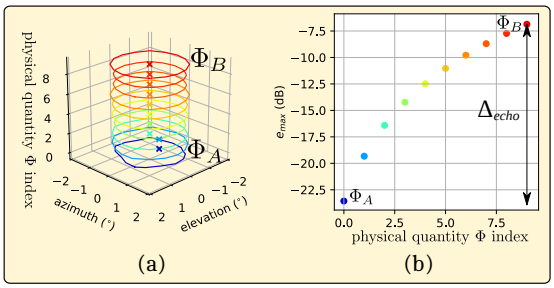

Fig. 4. (a) Simulated isolines in the plane (θ, φ) associated with the sensing scattering mode of a passive sensor, and for a physical quantity Φ varying from Φ_A to Φ_B ; (b) Statistical estimator e_{Max} defined as the maximal echo level inside each isoline from Φ_A to Φ_B.

III. Application to Zero-Power mm-Wave Sensors

We use here the commercially available FMCW radar DK-sR-1030e from IMST GmbH [36]. The carrier frequency f_C is of 23.8GHz and the bandwidth B is of 2GHz. The theoretical depth resolution $\frac{c}{2B}$ is then of 7.5cm. The output power is of 20dBm (100mW), and the Tx antenna is highly directive, with a beamwidth lower than 4°. The beamscanning is achieved here from mechanically scanning the Tx- and Rx-antennas in azimuth φ and elevation θ by using a pan-tilt. To illustrate the 3D radar imaging approach described in Section II, we first consider a passive target composed of (i) a horn antenna, (ii) a coaxial cable of electrical length L=1.2m, and (iii) a variable resistance. The echo level of this passive electromagnetic scatterer is expected to be dependent on the resistance value. The scatterer is located at 5.5m in front of the radar antennas. The resulting isolines are generated and displayed in Fig. 5(a) in the plane (θ, φ) for loading resistance ranging from 2.6Ω to 50Ω. The statistical estimator e_{Max} of each isoline is shown in Fig. 5(b). The large full-scale range Δ_{echo} of 17.8dB is measured. When the resistance takes values between 44Ω and 50Ω, the signal-to-noise-ratio is too low for remotely deriving the impedance value for the estimator e_{Max} and no isoline is generated. As reported in [35], other statistical estimators can be defined for enlarging the full-scale dynamic range, if required.

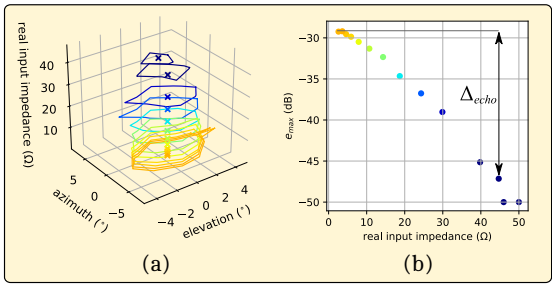

Fig. 5. (a) Isolines in the plane (θ, φ) associated with the sensing scattering mode of a passive scatterer (antenna loaded by a variable resistance) located at 5.5m in front of the radar and for different loading resistances; (b) Statistical estimator e_{Max} defined as the maximal echo level inside each isoline for resistances between 2.6Ω to 50Ω (matched impedance).

In a second experiment to perform the remote measurement

of a physical quantity from a 3D radar imaging approach, we used a fully passive on-the-shelf thermistor originally designed to work below 10 GHz [37]. A simple impedance matching circuit was added to obtain a passive temperature sensor working at 24GHz. This sensor was connected to a horn antenna through a transmission line, and finally illuminated by the radar imager at distance of 2.4m at five different temperatures. Isolines (see Fig. 6(a)) and the corresponding statistical estimator e_{Max} (see Fig. 6(b)) were computed at each temperature. The full-scale range Δ_{echo} of 4.4dB was obtained between 25.2°C to 55.2°C. This led to the sensitivity of 0.15dB/°C. The temperature resolution was of 1.3°C, that is, only 4.5% of the full-scale range.

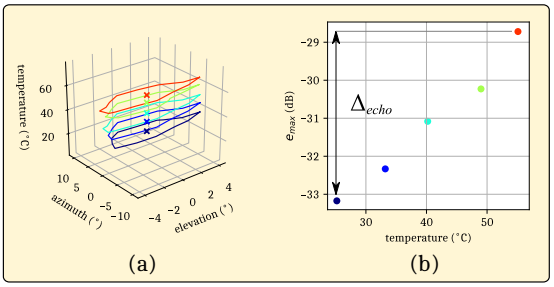

Fig. 6. (a) Isolines in the plane (θ, φ) associated with the sensing scattering mode of a passive scatterer (antenna loaded by a variable resistance) located at 5.5m in front of the radar and for different loading resistances; (b) Statistical estimator e_{Max} defined as the maximal echo level inside each isoline for resistances between 2.6Ω to 50Ω (matched impedance).

In the experiment reported in [18], [19], a fully passive microfluidic temperature sensor was placed at distance of 2.5m in front of the radar imager. The sensing scattering mode was located at 4.3m. The microfluidic channel crossed a 1mm-width microstrip line loaded by a 50Ω-matched impedance, and this channel was connected to a small tank filled with water. Due to the dilatation coefficient of the liquid, the water meniscus moved in the channel when temperature changed. For an empty gap (meniscus position at 0mm for low temperature), no transmission occurred through the gap and the echo level of the microfluidic sensor was high. For a completely filled gap (meniscus position at 1mm for higher temperatures), the transmission through the gap capacitance was generated, and the electromagnetic power was dissipated in the 50Ω-matched impedance. As a result, the echo level of the sensor was very small. Isolines of the sensing scattering mode for variable meniscus positions in the fluidic channel are displayed in Fig. 7(a). The statistical estimator e_{Max} for each isoline is displayed in Fig. 7(b). The large full-scale range Δ_{echo} of 6.3dB was obtained. This first result was very encouraging, even if the variation of the estimator e_{Max} with respect to the meniscus position deviated from a linear variation (the coefficient of determination R^2 of the linear regression was of 0.93 only). Since the echo level resolution was of 0.2dB, the minimal detectable displacement of the meniscus was of 40μm. The fact that it is possible to remotely measure such sub-millimeter fluid displacement by using a 24GHz (λ=1.25cm) FMCW radar reader is actually an interesting result.

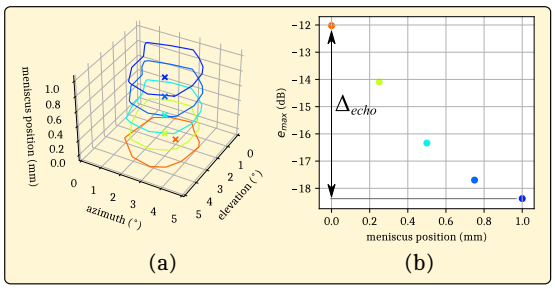

Fig. 7. (a) Isolines in the plane (θ, φ) computed from the sensing scattering mode of the passive microfluidic sensor located at 2.5m in front of the radar, and for five meniscus positions in the micro-channel; (b) Statistical estimator e_{Max} computed from isolines shown in Fig. 7(a).

In the next experiment [38], the passive humidity sensor reported in [39] was used. It consists of a 24GHz Van-Atta (retrodirective) and depolarizing patch antenna array. The sensor was printed on a Kapton substrate. The dielectric permittivity of this substrate is sensitive to the relative humidity and consequently, the resonant frequency of the patch antennas printed on the substrate surface changes as the humidity varies. When the resonant frequency belongs to the radar bandwidth, the echo level of the patch antenna array is high, while it is low when this frequency is outside the radar bandwidth. In order to mitigate the radar clutter, we measured the cross-polarized field backscattered by the humidity sensor when a co-polarized electromagnetic field was incident. The Tx-antenna of the radar was then co-polarized, while the Rx-antenna was cross-polarized. The passive humidity sensor was placed inside a closed Rohacell®box with a controlled relative humidity. The humidity sensor was located at 1.7m in front of the radar. In Fig. 8(a) are displayed isolines of the sensing scattering mode for variable relative humidity ranging from 38% to 69%. These isolines are computed only from the cross-polarized electromagnetic field backscattered by the sensor. The corresponding statistical estimator e_{Max} is shown in Fig. 8(b). The large full-scale range Δ_{echo} of 12.0dB was measured. We have shown in [40] that this passive sensor can be interrogated in an indoor environment (corridor) at the distance of 58m.

The last illustrative application reported here concerns the passive pressure sensor [23]. The sensor is composed of millimeter-wave microstrip resonator placed inside a cavity. The top of the cavity is a silicon membrane which deflects when a pressure is applied on its surface. This deflection causes the variation of the resonant frequency of the planar resonator. When the resonant frequency belongs to the radar bandwidth, the echo level of the sensor is low, while it is high when this frequency is outside the radar bandwidth. The passive pressure sensor is interrogated at a distance of 4.2m. By using a transmission line, the sensing scattering mode is placed at 5.4m. In Fig. 9(a) are displayed the isolines of the sensing scattering mode for applied pressure ranging from

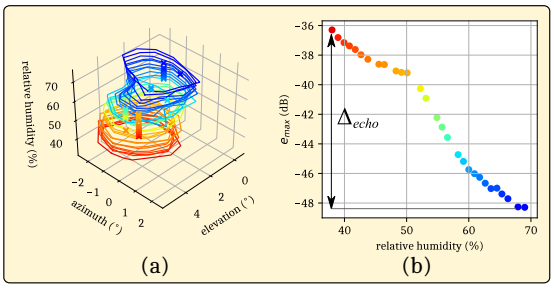

Fig. 8. (a) Isolines in the plane (θ, φ) computed from the sensing scattering mode of the passive humidity sensor located at 1.7m in front of the radar and for a relative humidity ranging from 38% to 69%; (b) Statistical estimator e_{Max} computed from isolines shown in Fig. 8(a).

0bar to 3bars. The statistical estimator e_{Max} of each isoline is displayed in Fig. 9(b) as a function of the pressure applied on the sensor membrane. We obtain a measured full-scale range of 9.2dB. This range is of 8.7dB between 0bar and 2bars for the sensitivity of 4.3dB/bar. Since the echo level resolution was of 0.2dB, the minimal detectable applied pressure is of 50mbars, that is, only 2.5% of the full-scale range. We have shown in [22] that this sensor can be interrogated in a highly reflective indoor environment at distances of few meters.

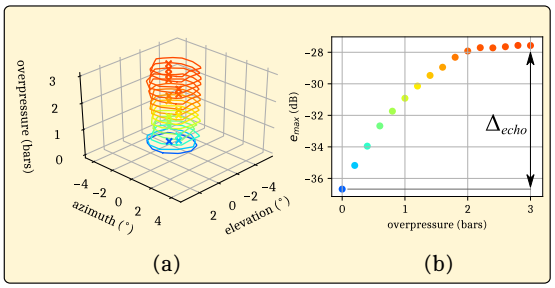

Fig. 9. (a) Isolines in the plane (θ, φ) computed from the sensing scattering mode of the passive pressure sensor located at 5.4m in front of the radar and for an applied pressure ranging from 0bar to 3bars; (b) Statistical estimator e_{Max} computed from isolines shown in Fig. 9(a).

IV. Conclusion

We have reported here a new radar technique for detecting and remotely analyzing passive, chipless and wireless sensors. Isolines have been computed from 3D radar images to derive physical quantities of interest. The technique can be used for on-fly measurement of moving passive sensors, as recently demonstrated in [40], and for reading passive sensors in reverberant environments from using dual-polarized passive repeaters [41].

References

[1] B. S. Cook, R. Vyas, S. Kim, T. Thai, T. Le, A. Traille, H. Aubert, M. M. Tentzeris, "RFID-Based Sensors for Zero-Power Autonomous, Wireless Sensor Networks," IEEE Sensors Journal, Vol. 14, No. 8, pp. 2419-2431, August 2014.

[2] H. Aubert, P. Pons, F. Chebila, M. M. Jatlaoui, " Measurement device comprising an electromagnetic diffuser," Patent Reference : WO2010/136388, 29 May 2009.

[3] M. M. Jatlaoui, F. Chebila, P. Pons, H. Aubert, " Pressure Sensing Approach Based on Electromagnetic Transduction Principle," Asia Pacific Microwave Conference, Hong Kong and Macao, China, 16-20 December 2008.

[4] E. Ozturk, D. Genschow, U. Yodprasit, B. Yilmaz, D. Kissinger, W. Debski, W. Winkler, "Measuring Target Range and Velocity: Developments in Chip, Antenna, and Packaging Technologies for 60-GHz and 122-GHz Industrial Radars", IEEE Microwave Magazine, vol. 18, no 7, pp. 26-39, Nov. 2017

[5] S. Thomas, C. Bredendiek, T. Jaeschke, F. Vogelsang, N. Pohl, "A compact, energy-efficient 240 GHz FMCW radar sensor with high modulation bandwidth," German Microwave Conference, Bochum, Germany, March 14-16, 2016.

[6] H. J. Ng, M. Kucharski, D. Kissinger, "Scalable sensor platform with multi-purpose fully-differential 61 and 122 GHz transceivers for MIMO radar applications," IEEE Bipolar/BiCMOS Circuits and Technology Meeting, New Brunswick, New Jersey, USA, 25-27 september 2016.

[7] D. Henry, H. Aubert, T. Véronèse, É. Serrano, "Remote Estimation of Intra-Parcel Grapes Quantity From Three-Dimensional Imagery Technique Using Ground-based Microwave FMCW Radar," IEEE Instrumentation and Measurement Magazine, Vol. 20, Issue 3, pp. 20-24, January 2017.

[8] D. Henry, H. Aubert, T. Véronèse, "Proximal Radar Sensors for Precision Viticulture," IEEE Transactions on Geoscience and Remote Sensing, vol. 57, no. 7, pp. 4624-4635, July 2019.

[9] D. Henry, H. Aubert, E. Ricard, D. Hazard, M. Lihoreau, "Automated Monitoring of Livestock Behavior Using Frequency-Modulated Continuous-Wave Radars," Progress In Electromagnetics Research M, Vol. 69, pp. 151-160, 2018.

[10] M. M. Jatlaoui, F. Chebila, P. Pons, H. Aubert, "Working Principle Description of the Wireless Passive EM Transduction Pressure Sensor," The European Physical Journal - Applied Physics, Vol. 56, Issue 1, Article 13702, October 2011.

[11] M. M. Jatloui, P. Pons, H. Aubert, "Radio-Frequency pressure transducer," 37th European Microwave Conference, München, Germany, pp.983-986, 8-12 October 2007.

[12] M. M. Jatloui, P. Pons, H. Aubert, "Pressure Micro-sensor based on Radio-Frequency Transducer," IEEE International Microwave Symposium, Atlanta, Georgia, USA, pp. 1203-1206, 15-20 June 2008.

[13] C. Arenas, J. Philippe, D. Henry, A. Rumeau, H. Aubert, P. Pons, "Wireless and Passive Nuclear Radiation Sensors," European Microwave Conference, Nuremberg, Germany, 9-13 October 2017.

[14] H. Hallil, P. Ménini, H. Aubert, "Novel Microwave Gas Sensor Using Dielectric Resonator with SnO2 Sensitive Layer", Eurosensors, Lausanne, Switzerland, 6–9 September 2009.

[15] T. Thai, M. M. Jatlaoui, H. Aubert, P. Pons, G. R. DeJean, M. M. Tentzeris, R. Plana, "A Novel Passive Wireless Ultrasensitive Temperature RF Transducer for Remote Sensing," IEEE International Microwave Symposium, Anaheim, California, USA, pp. 473-476, 23-28 May 2010.

[16] A. Traille, S. Bouaziz, S. Pinon, P. Pons, H. Aubert, A. Boukabache, M. M. Tentzeris, "A Wireless Passive RCS-based Temperature Sensor using Liquid Metal and Microfluidics Technologies," European Microwave Conference, Manchester, pp.45-48, 9-14 October 2011.

[17] T. Thai, M. M. Jatlaoui, F. Chebila, H. Aubert, P. Pons, G. R. DeJean, M. M. Tentzeris, R. Plana, "Design and Development of a Novel Passive Wireless Ultrasensitive RF Temperature Transducer for Remote Sensing," IEEE Sensors Journal, Vol. 12, Issue 9, pp. 2756-2766, September 2012.

[18] S. Bouaziz, F. Chebila, A. Traille, P. Pons, H. Aubert, M. M. Tentzeris, "Novel Micro-fluidic Structures for Wireless Passive Temperature Telemetry Medical Systems Using Radar Interrogation Techniques in Ka-band," IEEE Antennas and Wireless Propagation Letters, vol. 11, pp. 1706-1709, 2012.

[19] D. Henry, H. Aubert, P. Pons, J. Lorenzo, A. Lázaro, D. Girbau, "Novel technique for the wireless reading of passive microfluidic sensors," Electronics Letters, Vol. 54, No. 3, pp. 150–151, February 2018.

[20] T. Thai, H. Aubert, P. Pons, G. DeJean, M. M. Tentzeris, R. Plana, "Novel Design of a Highly Sensitive RF Strain Transducer for Passive and Remote Sensing in Two Dimensions," IEEE Transactions on Microwave Theory and Techniques, Vol. 61, Issue 3, pp. 1385-1396, March 2013.

[21] F. Chebila, M. M. Jatlaoui, P. Pons, H. Aubert, "Pressure Measurement from the RADAR Interrogation of Passive Sensors," IEEE Antennas and Propagation Symposium, Toronto, Ontario, Canada, 11-17 July 2010.

[22] J. Philippe, M. V. De Paolis, D. Henry, A. Rumeau, A. Coustou, P. Pons, H. Aubert, "In-Situ Wireless Pressure Measurement Using Zero-Power Packaged Microwave Sensors," Sensors, vol. 19, no 6, pp. 1263, March 2019.

[23] J. Philippe, D. Henry, M. V. De Paolis, A. Rumeau, A. Coustou, P. Pons, H. Aubert, "Wireless Remote Monitoring of Packaged Passive Sensor for In-situ Pressure Measurement in Highly Reflective Environments," IEEE International Microwave Symposium, Philadelphia, Pennsylvania, USA, 10-15 June 2018.

[24] M. M. Jatlaoui, F. Chebila, S. Bouaziz, P. Pons, H. Aubert, "Original Identification technique of passive EM Sensors using Loaded Transmission Delay Lines," European Microwave Week, Paris, France, 26 September – 1 October 2010.

[25] F. Chebila, M. M. Jatlaoui, P. Pons, H. Aubert, "Reconfigurable Multiband Scatterers for Micro-sensors Identification," IEEE AP-S International Symposium on Antennas Propagat., Charleston, South Carolina, USA, 1-5 June 2009.

[26] M. M. Jatlaoui, F. Chebila, P. Pons, H. Aubert, "New Micro-sensors Identification Techniques Based on Reconfigurable Multi-band Scatterers," Asia-Pacific Microwave Conference, Singapore, 7-10 December 2009.

[27] S. O. Piper, "Receiver frequency resolution for range resolution in homodyne FMCW radar," Telesystems Conference: Commercial Applications and Dual-Use Technology, pp.169-173, 16-17 June 1993.

[28] H. Aubert, P. Pons, M. M. Tentzeris, "Wireless Remote Sensing Based on Radar Cross Section Variability Measurement of Passive Electromagnetic Sensors," European Conference on Antennas and Propagation, Gothenburg, Sweden, pp.1714-1717, 8-12 April 2013.

[29] H. Aubert, F. Chebila, M. M. Jatlaloui, T. Thai, H. Hallil, A. Traille, S. Bouaziz, A. Rifai, P. Pons, P. Menini, M. M. Tentzertis, "Wireless Sensing and Identification based on RADAR Cross Sections Variability Measurement of Passive Electromagnetic Sensors," Annals of Telecommunications, Special Issue on Chipless RFID, Vol. 68, Issue 7-8, pp. 425-435, August 2013.

[30] D. Henry, A. Rifai, P. Pons, H. Aubert, "Millimetre-wave Scanning Radar for the Detection and Remote Reading of Passive Electromagnetic Sensors," 9th European Conference on Antennas and Propagation, Lisbon, Portugal, 12-17 April 2015.

[31] H. Aubert, P. Pons and D. Henry, "Wireless Detection, Identification and Reading of Passive Electromagnetic Sensors based on Beam-Steering FMCW Radar," 1st URSI Atlantic Radio Science Conference (URSI AT-RASC), Gran Canaria, 18-22 May 2015.

[32] D. Henry, P. Pons, H. Aubert, "3D Scanning Radar for the Remote Reading of Passive Electromagnetic Sensors," IEEE International Microwave Symposium, Phoenix, USA, 17-22 May 2015.

[33] D. Henry, P. Pons, H. Aubert, "3D Microwave Imaging System for the Remote Detection and Reading of Passive Sensors," European Microwave Conference, Paris, France, 7-10 September 2015.

[34] D. Henry, H. Aubert, "Isolines fin 3D radar images for remote sensing applications," European Microwave Conference, Paris, France, 29 September–4 October 2019.

[35] D. Henry, H. Aubert, P. Pons, "Wireless Passive Sensors Interrogation Technique Based on a Three-Dimensional Analysis," European Microwave Conference, London, UK, 3-7 October 2016.

[36] "Products – IMST Radar", [Online] Available: www.radarsensor.com/products/

[37] D. Henry, H. Aubert, P. Pons, "3D Scanning and Sensing Technique for the Detection and Remote Reading of a Passive Temperature Sensor," IEEE International Microwave Symposium, San Francisco, California, USA, 22-27 May 2016.

[38] D. Henry, J. Hester, H. Aubert, M. M. Tentzeris, P. Pons, "Long Range Wireless Interrogation of Passive Humidity Sensors using Van-Atta Cross-Polarization Effect and 3D Beam Scanning Analysis," IEEE International Microwave Symposium, Honolulu, Hawaii, USA, 4-9 June 2017.

[39] J. G. D. Hester and M. M. Tentzeris, "Inkjet-printed Van-Atta reflectarray sensors: A new paradigm for long-range chipless low cost ubiquitous smart skin sensors of the Internet of Things," IEEE MTT-S Int. Microw. Symp. Dig., San Francisco, CA, USA, May 2016, pp.1-4.

[40] D. Henry, J. G. D. Hester, H. Aubert, P. Pons and M. M. Tentzeris, "Long Range Wireless Interrogation of Passive Humidity Sensors using Van-Atta Cross-Polarization Effect and Different Beam Scanning Technique," IEEE Transactions on Microwave Theory and Techniques, Vol. 65, Issue 12, pp. 5345-5354, December 2017.

[41] T. Marchal, J. Philippe, D. Henry, M. V. De Paolis, A. Coustou, P. Pons, H. Aubert, "Millimetre-Wave Interrogation of Passive Sensors Embedded Inside Closed Reverberant Environments from Dual-Polarized Passive Repeaters," European Microwave Conference, Paris, France, 29 September-4 October 2019.